Approximate Micromechanics Treatise of Composite Impact

Christos C. Chamis and Louis M. Handler
Glenn Research Center, Cleveland, Ohio

The NASA STI Program Office . . . in Profile

Since its founding, NASA has been dedicated to the advancement of aeronautics and space science. The NASA Scientific and Technical Information (STI) Program Office plays a key part in helping NASA maintain this important role.

The NASA STI Program Office is operated by Langley Research Center, the Lead Center for NASA's scientific and technical information. The NASA STI Program Office provides access to the NASA STI Database, the largest collection of aeronautical and space science STI in the world. The Program Office is also NASA's institutional mechanism for disseminating the results of its research and development activities. These results are published by NASA in the NASA STI Report Series, which includes the following report types:

- TECHNICAL PUBLICATION. Reports of completed research or a major significant phase of research that present the results of NASA programs and include extensive data or theoretical analysis. Includes compilations of significant scientific and technical data and information deemed to be of continuing reference value. NASA's counterpart of peer-reviewed formal professional papers but has less stringent limitations on manuscript length and extent of graphic presentations.

- TECHNICAL MEMORANDUM. Scientific and technical findings that are preliminary or of specialized interest, e.g., quick release reports, working papers, and bibliographies that contain minimal annotation. Does not contain extensive analysis.

- CONTRACTOR REPORT. Scientific and technical findings by NASA-sponsored contractors and grantees.

- CONFERENCE PUBLICATION. Collected papers from scientific and technical conferences, symposia, seminars, or other meetings sponsored or cosponsored by NASA.

- SPECIAL PUBLICATION. Scientific, technical, or historical information from NASA programs, projects, and missions, often concerned with subjects having substantial public interest.

- TECHNICAL TRANSLATION. English-language translations of foreign scientific and technical material pertinent to NASA's mission.

Specialized services that complement the STI Program Office's diverse offerings include creating custom thesauri, building customized databases, organizing and publishing research results . . . even providing videos.

For more information about the NASA STI Program Office, see the following:

- Access the NASA STI Program Home Page at *http://www.sti.nasa.gov*

- E-mail your question via the Internet to help@sti.nasa.gov

- Fax your question to the NASA Access Help Desk at 301–621–0134

- Telephone the NASA Access Help Desk at 301–621–0390

- Write to:
  NASA Access Help Desk
  NASA Center for AeroSpace Information
  7121 Standard Drive
  Hanover, MD 21076

Approximate Micromechanics Treatise of
Composite Impact

Christos C. Chamis and Louis M. Handler
Glenn Research Center, Cleveland, Ohio

Available from

Approximate Micromechanics Treatise of Composite Impact

Christos C. Chamis and Louis M. Handler
National Aeronautics and Space Administration
Glenn Research Center
Cleveland, Ohio 44135

Summary

A formalism is described for micromechanic impact of composites. The formalism consists of numerous equations which describe all aspects of impact from impactor and composite conditions to impact contact, damage progression, and penetration or containment. The formalism is based on through-the-thickness displacement increments simulation which makes it convenient to track local damage in terms of microfailure modes and their respective characteristics. A flow chart is provided to cast the formalism (numerous equations) into a computer code for embedment in composite mechanic codes and/or finite element composite structural analysis.

Introduction

Composites in aerospace vehicles in general and composites in engine structures in particular are subjected to inadvertent and design-for impact loads. References [1-3] describe various types of impacts, approximate methods, while refs. [4-6] describe different experimental techniques to evaluate composite impact. References [7,8] describe impact damage in composite structures by classical formulations while refs. [9,10] describe impact damage in composite engine structures. Damage tolerance and dynamic loading in composites are extensively described in two recent books [11,12]. From those studies as well as others and continuing research on three-dimensional finite element simulations, it is fair to note that impact damage in composites is very complex and is mostly evaluated by testing [11-13].

The complexity arises from the multitude of composite fracture modes that are caused during impact and the attendant failure mechanisms associated with those fracture modes. Impact damage for specific designs can be evaluated by finite element simulations. However, local tracking of damage during impact and identification of local fracture modes is a very tedious and often an elusive process. Because the finite element model for composite impact is usually very large, it requires substantial personnel expertise and effort, and long computer times. Therefore it is cost prohibitive if not impossible to use finite element simulations in preliminary designs of composite structures for impact resistance. It is also fair to note that an inclusive micromechanics treatise of composite impact has not been developed or even proposed as yet [14-18]. The work reported in [14-15] is a step in that direction.

It is timely then to develop a micromechanics based generic and inclusive treatise of composite impact. The objective of this report is to describe the development of the formalism for a micromechanics treatise of composite impact. The treatise covers all aspects of impact damage from contact to penetration and includes cratering and spallation. It describes local damage as it occurs and the various fracture modes that are induced during the damage process. Strain rate effects are neglected because of the in situ three-dimensional constraints in the matrix. Only point impact is considered since it is assumed that this will be coupled with structural analysis for global response. Equations are derived for penetration time, residual velocity, rebound velocity and backface splitting. Equations are also derived for impact force-time trace and impact containment. A flow chart is outlined which cast the formalism into a computer module computational algorithm which can be made part of available composite mechanics codes and

general purpose finite element for composite structural analysis. Because of its inclusiveness and generality the treatise is approximate relative to mathematical rigor but consistent in the approximations with mechanics of materials approach.

Nomenclature

A	area
D	projector diameter
E	energy, modulus, E.E. elastic energy
F	force
G	shear modulus
g	gravitation constant
h	crater height
K	K.E. kinetic energy
M	moisture, mass
R	projectile radius, transformation array
r	contact area radius
S	strength
T	time, tension, temperature
t	thickness, time, t_ℓ ply thickness
V_{ind}	volume of indentation
v	velocity
z_p	projectile penetration depth
x,y,z	coordinate axis
α	thermal expansion coefficient
β	moisture expansion coefficient
ΔT	temperature change
ε	limit strain
$\in$	strain
θ	angle contact area periphery (figure 1), ply orientation angle (figure 6)
ℓ	laminate property
ν	Poisson's ratio
ρ	material density
Σ	summation
σ	stress
$\{\}, []$	vector, array, respectively

Subscripts

C	compression
c	laminate, contact crushing
crz	crz composite, rz direction
F	bending (flexural) fiber
i	indentation
o	initial property
p	projectile related, penetration
S	strength
s	shear
x,y,z	coordinate direction (figure 13)
$1,2,3$	material axes (1-along the fiber)

Some Geometric Relationships

Express the radius, r, and the angle, θ, of the contact area as a function of z the local indentation of an impactor with a spherical tip of radius R_p (figure 1).

$$\left(R_p - z\right)^2 + \left(r\right)^2 = R_p^2$$
$$R_p^2 - 2R_pz + z^2 + r^2 = R_p^2 \tag{2.1}$$
$$r^2 = 2R_pz - z^2 = z(2R_p - z)$$

$$r = \left[z\left(2R_p - z\right)\right]^{1/2} \tag{2.1a}$$

$$\theta = \sin^{-1}\left(\frac{r}{R_p}\right) = \sin^{-1}\left\{\frac{\left[z\left(2R_p - z\right)\right]^{1/2}}{R_p}\right\} \tag{2.2}$$

The volume of the spherical cap with radius r and depth z is derived as follows:

$$dV_{ind} = \pi r^2 dz$$
$$V_{ind} = \int_0^{V_{ind}} dV_{ind} = \int_o^z \pi r^2 dz \tag{2.3}$$
$$= \int_0^z \pi\left[2R_pz - z^2\right]dz$$
$$= \pi\left[R_pz^2 - \frac{1}{3}z^3\right]_o^z$$

$$V_{ind} = \pi\left[R_pz^2 - \frac{1}{3}z^3\right] = \frac{\pi z^2}{3}\left[3R_p - z\right] \tag{2.4}$$

Check for the volume of a hemisphere: $\dfrac{\pi D_p^3}{12}$

$$\frac{\pi D_p^3}{12} = \pi\left[\frac{D_p}{2}\left(\frac{D_p^2}{4}\right) - \frac{1}{3}\frac{D_p^3}{8}\right]$$

$$= \pi\left[\frac{D_p^3}{8} - \frac{D_p^3}{24}\right] = \frac{\pi}{24}\left[3D_p^3 - D_p^3\right]$$

$$\frac{\pi D_p^3}{12} = \frac{\pi D_p^3}{12} \qquad O.K.$$

Penetration Description

Penetration is a time dependent process. Here we consider very fast penetration that is the structure responds only locally by material damage (stress waves do not reach the boundaries).

The material getting indented is equal to the volume of the spherical cap in the indentation (figure 2). The energy required to crush this volume of material is given by

$$E_c = \frac{1}{2} V_{ind} S_{c33C} \tag{3.1}$$

Where E_c denotes the energy of indentation, V_{ind} is the crushed volume, and S_{c33C} is the flat-wise laminate strength. If we further assume that this equals the kinetic energy absorbed (relatively stiff indentor compared to composite flat-wise stiffness) a projectile with mass M_p, and an initial velocity v_o, then for energy conservations the kinetic energy of the projectile equals the energy expanded E_c to crush the material:

$$E_c = \left(\frac{1}{2} M_p v_o{}^2 \right)_p = \frac{1}{2} V_{ind} S_{c33C}$$

$$M_p v_o{}^2 = V_{ind} S_{c33C} \tag{3.2}$$

$$v_o = \left(\frac{V_{ind} S_{c33C}}{M_p} \right)^{1/2}$$

It is noted that v_o is the projectile velocity prior to contacting the target. Check units:

$$v_o = \left[\frac{in.^3 \; lb/in.^2}{in.^3 \; lb/in.^3 \; in./\sec^2} \right]^{1/2} = \left[\frac{in.^3 \; lb/in.^2}{lb/ \left(in/\sec^2 \right)} \right]^{1/2}$$

$$v_o = \left(in.^2 / \sec^2 \right)^{1/2} = in. / \sec$$

Therefore, the units check.

The next step is to assume that the projectile has first to crush the impacted surface up to its equator and beyond until the crushing force exceeds the remaining thickness shear-stress-resistance to push it through as a plug.

$$V_{ind} = \frac{1}{12} \pi D_p^3 \qquad \text{when} \qquad \left(z \le R_p \right) \tag{3.3}$$

$$V_{ind} = \frac{\pi D_p^3}{12} + \pi R_p^2 \left(z - R_p \right) \qquad \text{when} \qquad \left(z > R_p \right) \tag{3.4}$$

Equation (3.3) is half the spherical volume for a spherical projectile and equation (3.4) is that plus the volume of the shear plug figure 3. Then the crushing velocity required at $z > R_p$ and at $z \le R_p$ is given respectively by

$$v_c = \left[\frac{\left[\left(\frac{1}{12} \pi D_p^3 + \pi R_p^2 (z - R_p) \right) \right] S_{c33C}}{\frac{1}{6} \pi D_p^3 \rho_p / g} \right]^{1/2} \quad (z > R_p) \tag{3.5a}$$

$$= \left[\frac{2gz^2 (3R_p - z) S_{c33C}}{4 R_p^3 / \rho_p} \right]^{1/2} \quad (z \le R_p) \tag{3.5b}$$

Additional energy will be required to push the material ahead as a shear plug for penetration. That energy (E_s) is given by assuming the friction against the projectile is part of the shear resistance, figure 3 and the projectile velocity is v_s and the time t_s required during the shearing plug:

$$E_s = \frac{1}{2} S_{crzS} \left(\pi D_p t_s^2 \right) \qquad R_p \ge z_p \tag{3.6}$$

$$\frac{1}{2} M_p v_s^2 = \frac{1}{2} S_{crzS} \left(\pi D_p t_s^2 \right)$$

$$v_s = \left[\frac{\pi D_p t_s^2 S_{crzS}}{M_p} \right]^{1/2} \tag{3.7}$$

Another way to think is v_s is the projectile velocity the instant the shear block starts moving. For a spherical projectile of diameter D_p and for $M_p \ge$ than the mass of the plug:

$$M_p = \frac{\pi D_p^3}{6} (\rho / g)$$

$$v_s = \left[\frac{6 t_s^2 g S_{crzS}}{D_p^2 \rho_p} \right]^{1/2} = \left[\frac{in^2 \left(in / \sec^2 \right) lb / in^3}{in^2 \left(lb / in^3 \right)} \right]^{1/2} = \left(\frac{in^2}{\sec^2} \right)^{1/2} = \frac{in}{\sec} \quad \text{O.K.}$$

the units check.

The total velocity required for penetration E_p is calculated from the sum of the two energies

$$E_p = E_c + E_s$$

and the residual velocity is

$$v_p = \left[\frac{g(3z - R_p) S_{c33C}}{4 R_p \rho_p} + \frac{3 g t^2 S_{crzS}}{2 R_p \rho_p} \right]^{1/12} \tag{3.8}$$

It is noted that v_p is velocity that the projectile must have to crush and then start pushing the plug out. The residual velocity at the instant of v_p is E_r which is given by:

$$E_r = E_o - E_p = E_o - E_c - E_s$$

$$E_r = \frac{1}{2} M_p v_o^2 - \frac{1}{2} M_p v_c^2 - \frac{1}{2} S_{crzS} \pi D_p t_s^2$$

Dividing by M_p the equation for the residual velocity is

$$v_r = \left[v_o^2 - v_c^2 - \pi D_p t_s^2 \frac{S_{crzS}}{M_p} \right]^{1/2} \tag{3.9}$$

v_r is the residual velocity that drives the shear plug through, where v_o is the projectile initial velocity, v_c is the crushing velocity and the last term in the equation is the shear velocity.

Several points are worth observing:

1. $v_o = [v_c^2 + v_s^2]^{1/2}$: $v_r = 0$
2. $v_o > [v_c^2 + v_s^2]^{1/2}$: $v_r = [v_o^2 - (v_c^2 + v_s^2)]^{1/2}$
3. $v_o < [v_c^2 + v_s^2]^{1/2}$: Only partial penetration if at all.
4. For any velocity v_o and a given laminate with known S_{c33C} and S_{crzS}, a composite thickness t_c can be found for projectile containment.
5. Equivalently for a given t_c and S_{c33C}, an S_{crzS} can be selected for containment.

The equivalent force at the instant which the plug begins to move will be equal to the normal stress times the projected indentation surface area. For a spherical projectile at $z = R_p$ the surface area is:

$$A_{cs} = \frac{\pi D_p^2}{4}$$

and the force

$$F_c = A_{cs} S_{c33C} \tag{3.10}$$

$$F_c = \frac{1}{4} \pi D_p^2 S_{c33C} \tag{3.11}$$

This force or ratio thereof can then be used to perform evaluations for delaminations, splits and other fracture modes in the remaining laminate.

It is important to note that S_{crzS} very likely includes contributions from fiber fractures either in shear or in local bending. This implies that penetration will be dependent on the laminate configuration. It is suspected that delaminations and/or fiber crushing will occur when:

$$F_c = \frac{1}{4} \pi D_p^2 S_{c33C} > \pi D_p z S_{crzS} \qquad \left\{ \begin{array}{l} \text{interply strength} \\ \text{at that interply} \end{array} \right\}$$

$$F_c = \frac{1}{4} \pi D_p^2 S_{c33C} > \frac{1}{3} S_{crF} t_\ell^2 \qquad \left\{ \begin{array}{l} \text{Ply bending strength} \\ \text{at that intraply} \end{array} \right\} \tag{3.11a}$$

If fibers break in local bending the crushing force is

$$F_c = \frac{1}{3} S_{crF} t_\ell^2 \qquad (3.11b)$$

Where S_{crF} is the flexural strength and t_ℓ is the thickness of that ply, respectively.

Time to Penetration

Time to penetration (T_p) is the time required for the projectile to penetrate the laminate. That time can be estimated by assuming that the following relationship holds in an average sense:

$$\frac{1}{2} v_p T_p = t_p$$

$$T_p = \frac{2t_p}{v_p} \qquad (3.12)$$

where v_p is given in eq. (3.8) and t_p is the penetration thickness $(t_p = z)$. Since both v_o and v_p can be measured in a high-velocity-impact test, suitable tests can be conducted to verify eqs. (3.8) and (3.12) and indirectly eqs. (3.10), to (3.11b). It is noted here that equation (3.12) is only a rough estimate.

Cratering

Cratering occurs at the periphery of the contact as the material is pushed out due to high in-plane compressive stresses which are induced by the projectile ingress during crushing. The cratering is estimated by the following relationship (figure 4):

$$\varepsilon_{czz} = -v_{crz}\varepsilon_{crr}$$

$$\varepsilon_{czz} = -v_{crz} \frac{S_{c33C}}{E_{c33}} \qquad (3.13)$$

The crater height is determined from

$$h_{crater} = t_p \varepsilon_{czz} \qquad (3.14)$$

where t_p, v_{crz}, S_{c33C}, and ε_{c33} are evaluated at the depth of crushing at that time. Implicit in eq. (3.14) is that no cratering will occur once shearing started. The corresponding time is approximated:

$$\frac{1}{2} v_c T_c = t_p$$

$$T_c = \frac{2t_p}{v_c} \qquad (3.15)$$

where v_c is given by eq. (3.5). We can also determine whether spallation will occur as a result of cratering since we know the strain ε_{czz} at any $(t_p = z)$.

A condition for estimating spallation is given by

$$\sigma_{c33} > S_{c33T}$$

where s_{c33T} is given by

$$\varepsilon_{c33}E_{c33} = +\nu_{crz}S_{c33C}\frac{E_{c33}}{E_{c33}} = \nu_{crz}S_{c33C} > S_{c33T} \tag{3.16}$$

Delamination and Back Surface Splitting

These two conditions will occur if the penetration time is sufficiently long for shear waves to propagate in a region beyond projectile diameter. The shear stress waves velocities (v_{crz}) are given by

$$v_{crz} = \left(\frac{G_{crz}}{\rho_c}\right)^{1/2} \tag{3.17}$$

$$v_{cxy} = \left(\frac{G_{cxy}}{\rho_c}\right)^{1/2} \tag{3.18}$$

where G_{crz} and ρ_c are the corresponding laminate shear modulus and density, respectively. The distance these waves will travel at T_c are estimated by

$$\left.\begin{array}{l} r = v_{crz}T_c \\ x = y = v_{cxy}T_c \\ T_c = 2t_c / v_c \end{array}\right\} \tag{3.19}$$

Recall that t_p is the crushed thickness and v_c the corresponding velocity. Using the last equation in the above two equations and also eqs. (3.17) and (3.18) and by assuming average wall stress

$$\left.\begin{array}{l} r = \left(\dfrac{G_{crz}}{\rho_c}\right)^{1/2}\left(\dfrac{2t_c}{v_c}\right) \\ x = y = v_{cxy}T_c \\ \text{where} \quad v_p = \left[\dfrac{g\left(D_p^3 + 3R_p^2\left(z - R_p\right)\right)}{2D_p^3\rho_p}S_{c33C} + \left(g\dfrac{6t_s^2 S_{crzS}}{D_p^2\rho_p}\right)\right]^{1/2} \end{array}\right\} \tag{3.20}$$

Delamination will occur if:

$$
\left.\begin{array}{c}
r > D_p / 2 \\[2mm]
and \quad \dfrac{1}{4} D_p S_{c33C} > t_s S_{crzS}
\end{array}\right\}
\tag{3.21}
$$

and back surface splitting will occur if in addition to eq. (3.21) the following conditions hold:

$$
\frac{1}{4}\pi D_p^2 S_{c33C} > \frac{1}{3} t_\ell^2 S_{c22T} \left(\begin{array}{c} \text{tranverse} \\ \text{ply} \\ \text{splitting} \end{array}\right)
$$

$$
\frac{1}{4}\pi D_p^2 S_{c33C} > \frac{1}{3} t_\ell^2 S_{c11F} \left(\begin{array}{c} \text{longitudinal} \\ \text{fiber} \\ \text{breakage} \end{array}\right)
\tag{3.22}
$$

Note that the r in eq. (3.21) indicates an average radial stress wave velocity propagation. Values for r_x and r_y are calculated from

$$
\left.\begin{array}{l}
r_x = x = \left(\dfrac{G_{c\theta r}}{\rho_c}\right)^{1/2} T_c \cos\theta \\[4mm]
r_y = y = \left(\dfrac{G_{c\theta r}}{\rho_c}\right)^{1/2} T_c \sin\theta
\end{array}\right\}
\tag{3.23}
$$

where the x and y are the in-plane coordinates. These equations will give an elliptical wave propagation front, in general.

Thickness Growth

This growth is due to Poisson's effect. The ply in-plane unrestrained strains along the material axes are

$$
\{\varepsilon_\ell\} = \{\varepsilon_{\ell\,\mathrm{m}}\} + \Delta T \{\alpha_\ell\} + M \{\beta_m\}
\tag{4.1}
$$

Those in the in situ laminate are

$$
\{\varepsilon_\ell\} = [R_{\ell/\varepsilon}]\{\varepsilon_c\}
\tag{4.2}
$$

The ply in-plane restrained strains are the difference between eqs. (4.2) and (4.1)

$$
\{\varepsilon_\ell^R\} = [R_{\ell/\varepsilon}]\{\varepsilon_c\} - \{\varepsilon_\ell\}
\tag{4.3}
$$

The thickness growth is obtained by multiplying eq. (4.3) by the appropriate ply Poisson's ratios

$$\varepsilon_{izz} = \left[\nu_{\ell j3} \right] \left\{ \varepsilon_\ell^R \right\} \qquad\qquad j=1 \text{ and } 2 \qquad\qquad (4.4)$$

The composite or laminate thickness strain then is obtained from

$$\varepsilon_{czz} = \frac{1}{t_c} \sum_{i=1}^{N_\ell} \left(t_{\ell i} \varepsilon_{izz} \right) \qquad\qquad (4.5)$$

and the laminate change in thickness is obtained from

$$\Delta t_c = \sum_{i=1}^{N_\ell} \left(t_{\ell i} \varepsilon_{izz} \right) \qquad\qquad (4.6)$$

It is noted that these strains are in addition to those produced by impact. It should also be noted the ply in-plane strains are already known from laminate analysis. To obtain the thickness strains and thickness changes use the ply strains from laminate analysis in eq. (4.4) and proceed with eqs. (4.5) and (4.6).

Elastic Indentation Stresses

For an elastic indentation of depth Z, we assume continuous contact between projectile surface and target indentation. For this case, the in-plane and thickness-size local strains are uniform and the stresses will be proportional the local stiffness. Since the strains are uniform and the deformation conforms to the projectile surface, then at a depth Z it follows that the in-plane (ε_{crr} and $\varepsilon_{c\theta\theta}$) and thickness-wise ($\varepsilon_{czz}$) strains are:

$$\left.\begin{aligned} \varepsilon_{crr} &= \frac{\Delta r}{r} \\[1em] \varepsilon_{c\theta\theta} &= \left(1 + \frac{\Delta r}{r} \right) \\[1em] \varepsilon_{czz} &= \frac{\Delta z}{z} \end{aligned}\right\} \qquad\qquad (5.0)$$

Note eq. (5.0) denotes completely recoverable indentation. Note also that for a spherical indentor at any z, $r = [z(2R_p - z)]^{1/2}$, eq. (2.1a) and $q = \sin^{-1} r/R_p$. Then, the in-plane ply strains along the material axis are given by (see figure 5)

$$\left\{ \varepsilon_\ell \right\} = \left[R_{\varepsilon/\theta} \right] \left\{ \varepsilon_{cr} \right\} \qquad\qquad (5.1a)$$

$$\left\{ \begin{array}{c} \varepsilon_{11} \\ \varepsilon_{22} \\ \varepsilon_{12} \end{array} \right\} = \begin{vmatrix} \cos^2\theta & \sin^2\theta & \dfrac{1}{2}\sin 2\theta \\ \sin^2\theta & \cos^2\theta & \dfrac{1}{2}\sin 2\theta \\ -\sin 2\theta & \sin 2\theta & \cos 2\theta \end{vmatrix} \left\{ \begin{array}{c} \varepsilon_{crr} \\ 0 \end{array} \right\} \tag{5.1b}$$

The corresponding stresses are given by

$$\{\sigma_\ell\} = [E_\ell]\{\varepsilon_\ell\} \tag{5.1c}$$

where E_ℓ is defined by:

$$\left\{ \begin{array}{c} \sigma_{\ell 11} \\ \sigma_{\ell 22} \\ \sigma_{\ell 12} \end{array} \right\} = \begin{bmatrix} \dfrac{E_{\ell 11}}{1-\nu_{\ell 12}\nu_{\ell 21}} & \dfrac{-\nu_{\ell 21}E_{\ell 22}}{1-\nu_{\ell 12}\nu_{\ell 21}} & 0 \\ -\dfrac{\nu_{\ell 12}E_{\ell 11}}{1-\nu_{\ell 12}\nu_{\ell 21}} & \dfrac{E_{\ell 22}}{1-\nu_{\ell 12}\nu_{\ell 21}} & 0 \\ 0 & 0 & G_{\ell 12} \end{bmatrix} \left\{ \begin{array}{c} \varepsilon_{\ell 11} \\ \varepsilon_{\ell 22} \\ \varepsilon_{\ell 12} \end{array} \right\} \tag{5.1d}$$

Concisely the in-plane strains are given by

$$\{\varepsilon_{c\ell}\} = \left[R_{\varepsilon/\theta}\right]_\ell \{\varepsilon_{cr}\} \tag{5.2}$$

and the flat-wise

$$\{\varepsilon_{z\ell}\} = \left[R_{\varepsilon/z}\right]_\ell \{\varepsilon_{cz}\} \tag{5.3}$$

A more direct approach will be to obtain the three-dimensional strains from the three-dimensional transformation (see appendix A).

$$\{\varepsilon_{z\ell}\} = \left[R_{\varepsilon/r,\theta}\right]_\ell \{\varepsilon_{cz,z}\} \tag{5.4}$$

The last equation will provide all 6-strains from which the corresponding stresses can be obtained from the three-dimensional stress/strain relationships:

$$\{\sigma_{z\ell}\} = \left[E_{c\ell}\right]\{\varepsilon_{z\ell}\} \tag{5.5}$$

$$s = \left(\frac{\pi}{4k_f}\right)$$

Equations (5.4) and (5.5) can be evaluated by incrementing eq. (5.3) by a single fiber cell and continuously checking fracture modes. Here s is the edge of a fiber square array, k_f is the fiber volume ration and d_f is the fiber diameter. The strains fracture modes are obtained from

$$\{\varepsilon_{z\ell}\} \le \{\varepsilon_\ell\} \tag{5.6}$$

and the stresses fracture modes from

$$\{\sigma_{z\ell}\} \le \{S_\ell\} \tag{5.7}$$

If eqs. (5.6) or (5.7) are violated failure will occur by that fracture mode and permanent damage will be induced in the composite target at that location. Crushing will proceed as described in Penetration Description section.

The elastic energy stored down to depth z will be given by

$$E.E. = \frac{1}{2} \sum_{\Delta z=0}^{z} \lfloor \varepsilon_{z\ell} \rfloor \{\sigma_{z\ell}\} \pi r^2 \Delta z \tag{5.8}$$

where Δz is the thickness increment and r is evaluated at z from eq. (2.1a), in the section titled Some Geometric Relationship.

The loss in kinetic energy then is

$$(K.E.)_{loss} = E.E. \tag{5.9}$$

when

$$\{\sigma_{z\ell} \le S_\ell\} \tag{5.10}$$

No damage will occur and the projectile will bounce (rebound) with velocity equal to its initial velocity assuming no losses due to local heat or vibrations. To assure no heat and no vibration the contact time will have to be relatively small so that the change in local temperature is negligible:

$$\Delta T \approx 0 \tag{5.11}$$

where the impact surface temperature and the shear stress waves have not propagated beyond the a distance t_p (crushed thickness). The contact time for no damage can be evaluated from the rebound condition

$$\frac{1}{2}(v_o - 0)T_c = z \tag{5.12}$$

$$T_c = \frac{2z}{v_o} \tag{5.13}$$

Assuming an initial velocity of 30.5 m/sec (100 ft/sec) and an elastic indentation of $z \approx 0.013$ cm (0.005 in.) without damage in any fracture mode

$$T_c = \frac{2(0.005)}{1200} = \frac{0.010}{1200} \approx \frac{1.0}{1.2} \times 10^{-5} \text{ sec} \approx 8.33 \mu s$$

a very small time indeed.

Also the contact time for onset of damage can be calculated from eq. (5.8) by setting

$$E.E._{\cdot(\sigma_{z\ell} \geq S_{z\ell})} = \sum_{\Delta z}^{\overset{z}{}} \lfloor \varepsilon_{z\ell} \rfloor \{\sigma_{z\ell}\} \, dz \qquad (5.14)$$

These simplified equations can be readily checked by using available experimental data [3-5, 12 and 13]. Note that the aforementioned derivations are for hard object projectile. They need to be modified for soft impact. In that case the z increment will be on the projectile and r on the projectile flattening.

The other important point to note is that the energy for elastic deformation must be added to that for crushing and penetration if it is rather significant, say, more than 3 percent of their sum.

Force-Time Trace

The force time trace can be determined for both elastic impact and penetration impact. Elastic Impact—elastic indentation the force at any local indentation z is obtained from (figure 6).

$$F_z \approx \pi r^2 \sigma_{\ell zz} \qquad (6.1)$$

where r is given by

$$r = \left[z(2R_p - z) \right]^{1/2} \qquad (6.2)$$

and $\sigma_{czz\ell}$ is given by

$$\sigma_{\ell zz} = \frac{z}{t_c} E_{\ell 33} \qquad (6.3)$$

and the corresponding time is given by

$$T_z = \frac{2z}{v_o + v_z} \qquad (6.4)$$

where v_o is the projectile velocity at initial contact and v_z is determined from $(K.E.—E.E.)$ is satisfied or equivalently from the equation:

$$\frac{1}{2} M_p v_z^2 = \frac{1}{2} M_p v_o^2 - E.E.(z) \qquad (6.5)$$

Unloading will be obtained by deincrementing z and the contact time will be obtained from z max which occurs when $v_z = 0$ or from eq. (6.5):

$$E.E.(z_{\max}) = \frac{1}{2} M_p v_o^2.$$

Impact Damage Response

Impact damage response is evaluated by accounting for the energy expanded as impact damage progresses and accumulates (figure 7). The impact force is

$$F_z^{(1)} = \pi r^2 \sigma_{czz} \tag{7.1}$$

$$F_z^{(2)} = \pi r^2 S_{c33C} \tag{7.2}$$

$$F_z^{(3)} = 2\pi R_p t_c S_{crzS} \tag{7.3}$$

$$F_z^{(4)} = 0 \tag{7.4}$$

The corresponding times are given by:

$$T_z^{(1)} = 2z / (v_o + v_z) \tag{7.5}$$

$$\text{where} \quad \frac{1}{2} M_p v_z^2 = \left[\frac{1}{2} M_p v_o^2 - E.E. \right] \text{ (eq. (5.8), until } \sigma_{z\ell} = S_{\ell 33C}); \tag{7.6}$$

$$T_z^{(2)} = 2z / (v_o + v_z) \tag{7.7}$$

$$\text{where} \quad \frac{1}{2} M_p v_z^2 = \left[\frac{1}{2} M_p v_o^2 - E_2 \right] (E_2, \text{ eq. (3.2), } \ni \text{ shearing takes place}); \tag{7.8}$$

from the moment that crushing begins until the moment of transition from crushing to shear plug movement, or from the moment that $\sigma_{22\ell} = s_{\ell 33}$ to the moment $F_z^{(3)} \leq F_z^{(2)}$; where z_c is the penetration depth at the moment crushing ends; and v_z is the projectile's velocity at that same moment.

$$T_z^{(3)} = 2z_c / (v_o + v_z) + \frac{2(z - z_c)}{v_z + v_z} \tag{7.9}$$

$$\text{where} \quad \frac{1}{2} M_p v_z^2 = \left[\frac{1}{2} M_p v_o^2 - E_s \right] (E_s \ni \text{ due to shear}); \tag{7.10}$$

$$T_z^{(4)} = \frac{2z_c}{v_o + v_z} + \frac{2(t_c + R_p - z_c)}{v_z + v_e} \tag{7.11}$$

where t_c is the composite target thickness and where v_e is the exit velocity obtained from equation (7.10).

Computation Simulation

The penetration process can be simulated as described below. We can use the previous simple equations to computationally simulate the penetration process: The block diagram in figure 8 is one way to implement the impact process described, by the equations in the previous sections.

Typical Results

Typical results were obtained by using the computer module generated from the block diagram (flowchart) in figure 8 in conjunction with a composite mechanics computer-programmed [19] and reprogrammed, respectively in JAVA computer language code. These results are from assuming a hybrid $[0/90/0]_s$ laminate where the 0°-plies are AS graphite-fiber epoxy-matrix and the 90°-intraply hybrid plies are AS graphite-fiber epoxy-matrix// S-glass-fibers/epoxy-matrix composites. The constituent properties used are typical for these composites. The results are for three different initial velocities 36.6 m/sec (120 ft/sec), 366 m/sec (1200 ft/sec), and 3660 m/sec (12000 ft/sec). The projectile is a 0.64 cm (0.25 in.) diameter steel ball.

The force-time traces developed during impact and predicted by eqs. (7.1) through (7.4) are shown in figure 9. Three points are well worth observing: (1) the impact duration for each velocity, (2) projectile containment, and (3) laminate penetration. The locations for the projectile progression predicted by eq. (7.5) through (7.11) are shown in figure 10. Note containment for the two low velocities and early penetration for the highest. The velocity trace predicted by eq. (7.9) is shown in figure 11. Note the containment velocity is zero for the two low velocity impacts and very high residual (escape) velocity (about 90 percent retention) for the high velocity. The interply and intraply stresses develop during impact predicted by eqs. (3.11a) and (6.3) are shown in figure 12. Note that the lowest velocity reached only 69 Mpa (10 ksi) while both the others reached about 110 Mpa (16 ksi) denoting most likely interply and intraply delaminations for both of these. It is worth noting that the discontinuities in stresses shown in figure 12 are from the assumption that the in-plane strains are continuous prior to damage. Suffice it to say that this type of the laminate local detail can only be obtained by a micromechanics impact treatise such as described herein.

Conclusions

An investigation was performed to develop an approximate formalism for describing composite damage due to impact. The formalism consists of numerous composite micromechanic equations describing all aspects of impact from initial conditions (projectile, target) to containment and/or penetration. These equations describe damage initiation, damage progression and accumulation in terms of microfracture and respective fracture modes. Equations are also included for impact-force/time history and time to penetration as well as conditions for back surface splitting. A flow chart is outlined to cast the formalism in a computer code module for embedment in composite mechanics codes. The formalism in essence constitutes an approximate treatise of micromechanics for composite impact. Results obtained from the computer module of this flow chart illustrate laminate local detail information that can be generated. The three velocities investigated may be characterized as follows: crushing initiation, extensive crushing, and hyper velocity impact.

Appendix A

The three-dimensional strain transformations are given by the equations below where ℓ, m, n are direction defined by the table below (figure A1).

$$
\left.
\begin{aligned}
\varepsilon_{cxx} &= \ell_1^2 \varepsilon_{crr} + m_1^2 \varepsilon_{c\theta\theta} + n_1^2 \varepsilon_{czz} \\
\varepsilon_{cyy} &= \ell_2^2 \varepsilon_{crr} + m_2^2 \varepsilon_{c\theta\theta} + n_2^2 \varepsilon_{czz} \\
\varepsilon_{czz} &= \ell_3^2 \varepsilon_{crr} + m_3^2 \varepsilon_{c\theta\theta} + n_2^2 \varepsilon_{czz} \\
\\
\varepsilon_{cxy} &= 2\ell_1\ell_2 \varepsilon_{crr} + 2m_1 m_2 \varepsilon_{c\theta\theta} + 2n_1 n_2 \varepsilon_{czz} \\
\varepsilon_{cyz} &= 2\ell_2\ell_3 \varepsilon_{crr} + 2m_2 m_3 \varepsilon_{c\theta\theta} + 2n_2 n_3 \varepsilon_{czz} \\
\varepsilon_{czx} &= 2\ell_3\ell_1 \varepsilon_{crr} + 2m_3 m_1 \varepsilon_{c\theta\theta} + 2n_3 n_1 \varepsilon_{czz}
\end{aligned}
\right\}
\tag{A1}
$$

r, q, and z are attached to the projectile tangential plane and x, y, z are the laminate global axis. The undamaged ply stresses in the laminate at that point are obtained by: first, calculating the ply strains $e_{\ell 11}$, $e_{\ell zz}$, and $e_{\ell 23}$ along the material axis and second, by using the three-dimensional stress/strain relationships. The flat-wise (normal) ply stress $s_{\ell zz}$ is obtained by multiplying e_{czz} by $E_{\ell 33}$ and the flat-wise ply shear stress from

$$
\sigma_{\ell zz}^{(i)} = \left(\varepsilon_{czz} E_{\ell 33} \right)_i
\tag{A2}
$$

are obtained from

$$
\left.
\begin{aligned}
\sigma_{\ell yz} &= \varepsilon_{cyz} G_{\ell yz} \\
\sigma_{\ell zx} &= \varepsilon_{ezx} G_{\ell zx}
\end{aligned}
\right\}
\tag{A3}
$$

The interlaminar stresses are obtained from (assuming isotropic interply layer behavior)

$$
\left.
\begin{aligned}
\sigma_{izz}^{(j)} &= \left(\varepsilon_{czz} E_m \right)_j \\
\sigma_{iyz}^{(j)} &= \left(\varepsilon_{cyz} E_m \right)_j \\
\sigma_{izx}^{(j)} &= \left(\varepsilon_{czx} E_m \right)_j
\end{aligned}
\right\}
\tag{A4}
$$

In eq. (A4) i denotes interlaminar and j denotes the jth interlaminar layer.

Equations (A1) to (A4) are then compared to their corresponding strengths to identify local fractures and respective fracture modes. It is noted that eqs. (A1) to (A4) are general and can treat any material including isotropic hybrids and combinations. Thermal, moisture and residual stresses can be included as is done in the conventional laminate analysis. For local damage and progressive fracture the projectile induced strains are obtained by the incremental growth during the current time increment.

References

1. Anon., "Foreign Object Impact Damage to Composites," ASTM STP 568, American Society for Testing and Materials, 1975.
2. Greszczuk, L.B. and Chao, H., "Impact Damage in Graphite-Fiber-Reinforced Composites," Composite Materials: Testing and Design (Fourth Conference), ASTM STP 617, American Society for Testing and Materials, 1977, pp. 389–408.
3. Sun, C.T., "An Analytical Method for Evaluation of Impact Damage Energy of Laminated Composites," Composite Materials: Testing and Design (Fourth Conference), ASTM STP 617, American Society for Testing and Materials, 1977, pp. 427–440.
4. Lagace, P.A. and Wolf, E., "Impact Damage Resistance of Several Laminated Material Systems," AIAA Journal, vol. 33, no. 6, June 1995, pp. 1106–1113.
5. Habib, S.S., "Impact Response of Glass Fibre Reinforced Composite Plates," Journal of Reinforced Plastics and Composites, vol. 14, August 1995, pp. 799–803.
6. Gross, X.E., "Characterization of Low Energy Impact Damages in Composites," Journal of Reinforced Plastics and Composites, vol. 15, March 1996, pp. 267–282.
7. Moon, F.C., "Impact of Composite Plates, Analysis of Stresses and Forces," NASA CR–134999, Princeton, University, 1976.
8. Sih, G., "Normal and Radial Impact of Composites with Embedded Penny-Shaped Cracks," NASA CR–159538, Lehigh University, 1979.
9. Alexander, A. and Cornell, R.W., "Interactive Multi-Mode Blade Impact Analysis," NASA CR–159462, Hamilton Standard, 1978.
10. Lee, C.H., "CELF Coupled Eulerian-Lagrangian Finite Element Program for High Velocity Impact, Part I Theory and Formulations," NASA CR–159395, Lockheed Missiles and Space Company, 1978.
11. Scaproni, C. et al., "Reduction of Tensile Strength in Angle-Ply Composite Laminates Due to Low Velocity Impact," Journal of Reinforced Plastics and Composites, vol. 18, no. 01, 1999.
12. Cantwell, W.J., and Morton, J., "Comparison of the Low and High Velocity Impact Response of CFRP," Composites, vol. 20, pp. 545–551, 1989.
13. Morton, J., and Godwin, E.W., "Impact Response of Tough Carbon Fibre Composites," Composite Structures, vol. 13, pp. 1–19, 1989.
14. Sierakowski, R.L., and Newaz, G.M., "Damage Tolerance in Advanced Composites," Technomic Publishing Co., Lancaster, PA, 1995.
15. Sierakowski, R.L., and Chaturvedi, S.K., "Dynamic Loading and Characterization of Fiber-Reinforced Composites," John Wiley and Sons, New York, NY, 1997.
16. Langlie, S., and Cheng, W., "Numerical Simulation of High Velocity Impact on Fiber-Reinforced Composites," ASME Pressure Vessels and Piping Division (Publication) PVP., ASME, vol. 159, pp. 51–64, 1989.
17. Langlie, S., and Cheng, W., "A High Velocity Impact Penetration Model for Thick Fiber-Reinforced Composites," ASME Pressure Vessels and Piping Division (Publication) PVP., ASME, vol. 174, pp. 151–158, 1989.
18. Anon., "Impact Damage Tolerance Modelling of Composite Materials and Structures," Euromech Colloquium 400, Imperial College, London, United Kingdom, September 27–29, 1999.
19. Murthy, P.L.N., Ginty, C.A., and Sanfeliz, J.G., "Second Generation Integrated Composite Analyzer (ICAN) Computer Code," NASA TP–3290, 1993.
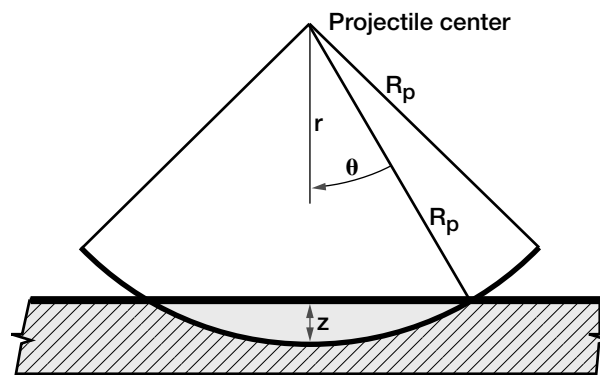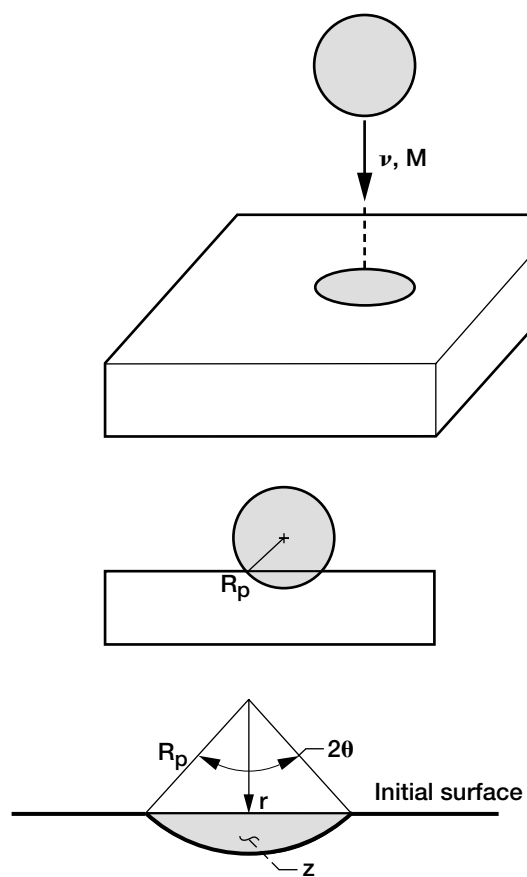
Figure 1.—Spherical indenter-portion diagram.

Figure 2.—Indentation diagram.

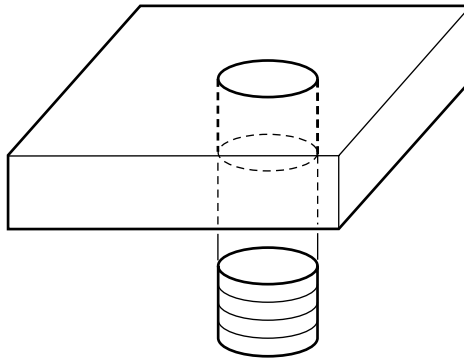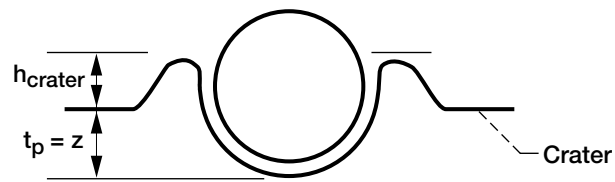Figure 3.—Penetration diagram.
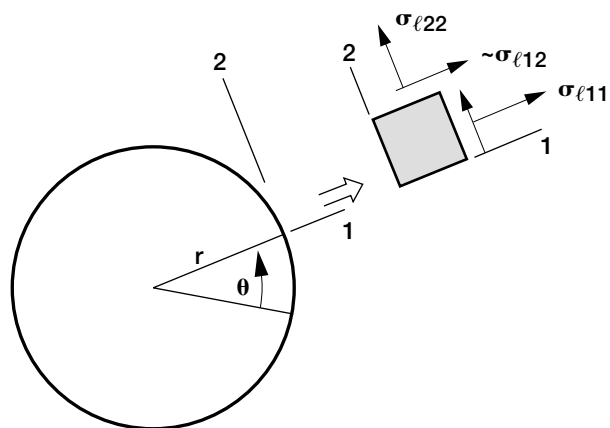

Figure 4.—Cratering diagram.
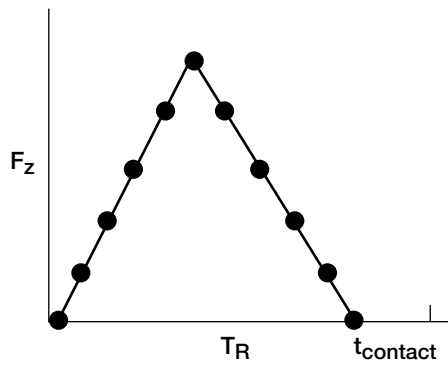

Figure 5.—Ply-stress transformation diagram.

Figure 6.—Impact force history diagram.

Figure 7.—Impact damage response.

1) Input:
Targe F.E. Model
Impactor F.E. Model
and initial cond

2) Select impact
region and
model as shown

3) Use composite
Mech to synthesize
laminate properties

4) Initialize at contact
$T = 0$, $z = 0$
$Ez = ra\, \mu 2/2$
$h = 0$

5) Calculate
$dz = \min\{tc, R_p\}/$
n increments

6) Increment z

7) Compute crushing
force Fz 3.11

8) Integrate to get
remaining energy
$Ez = Ez'-Fz\,dz$

9) If $Ez < 0$, set
$Ez = 0$

10) Calculate
V_{ind} (Eq. 2.4)

11) Velocity:
$v = \sqrt{[2\, Ez/Mp]}$

12) $dT = dz/v$

13) Integrate time:
$T = T' + dt$

14) Integrate crater
height: h crater =
h crater' + epslzz
dz

15) Test for failure
modes

16) If $v = > 0$
and
$z < R_p$ loop → back to 6

Completed initial crushing in
shape of projectile. Continue
crushing with cylindrical walls.

17) If v is zero skip
to print at end → [40]

18) Increment z

19) Compute crushing
force Fz

20) Compute shear
force Fb to push
out as a plug

21) If shear force <
crushing force
start push

22) $Ez = Ez'-Fz\,dz$

23) If $Ez < 0$, set
$Ez = 0$

24) $v = \sqrt{[2\, Ez/Mp]}$

25) $dT = dz/v$

26) $T = T' + dT$

27) Test for failure
modes

28) If $v > 0$ and $z <$
thickness + R_p
loop back to 18

29) If v is zero $z =$
thickness + R_p
skip to print at
end

30) $Ez = Ez'-EzDrop$
Where EzDrop =
Fz (thickness + Rp-
z chg) (? see 3.6)

31) If $Ez < 0$, $Ez = 0$,
If $v = 0$, skip to
print → [40]

Fz = Fb

z chg = z

If v is zero

skip to
print at end or
$z =$ thickness + R_p

32) $FzX = \mu\, Fz$ (friction
force)

33) Increment z

34) $Fz = FzX$ (thickness
+ R_p-z)/(thickness +
R_p-z chg)

35) $Ez = Ez'-Fz\,dz$

36) If $Ez < 0$, set
$Ez = 0$

37) $v = \sqrt{\dfrac{[2\, Ez/(Mp + \dfrac{\pi D_p^2\, tc\, \rho c)]}{4}}}$

38) $dT = dz/v$

39) $T = T' + dT$

40) If $v > 0$ and $z <$
thickness + R_p
loop back to 32

41) Print out
summary

42) Print out
per user specs
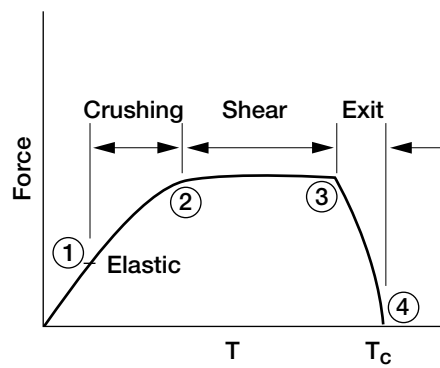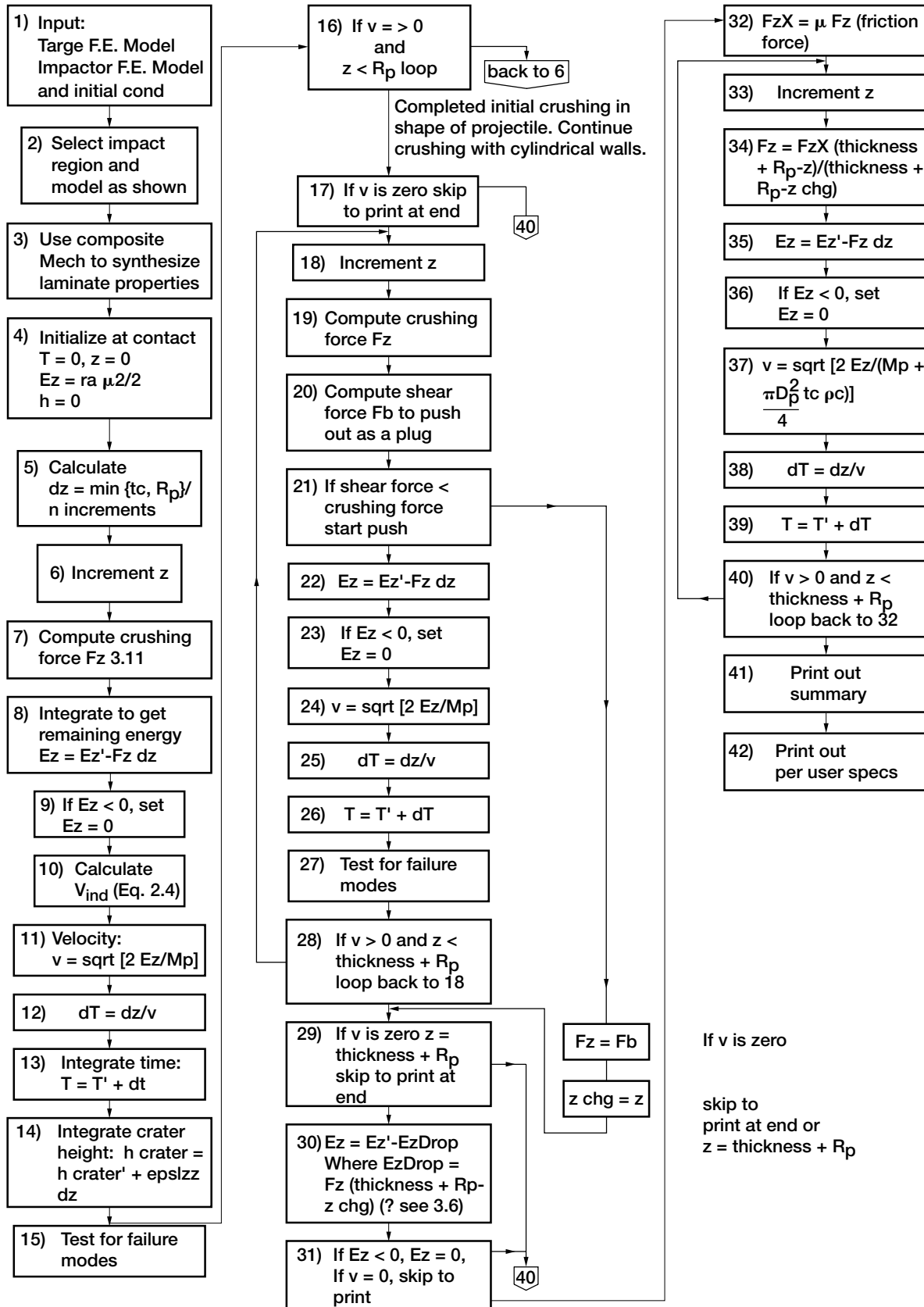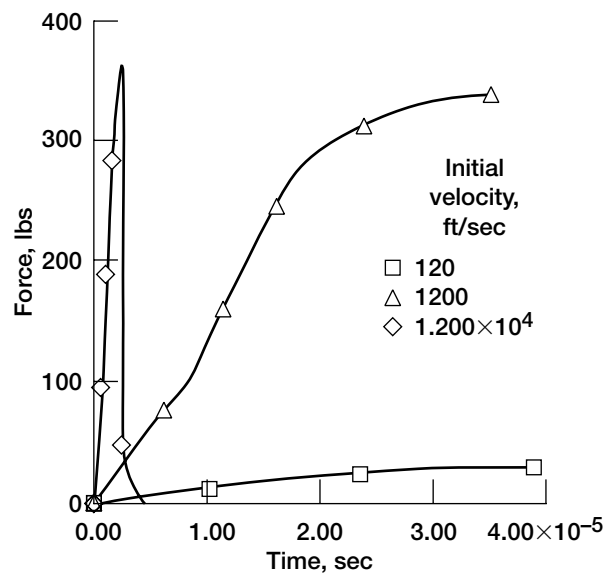
Figure 8.—Computational simulation flow chart.

Figure 9.—Impact force developed in a [0/90/0]$_s$
interply hybrid laminate (90°-plies intraply hybrid
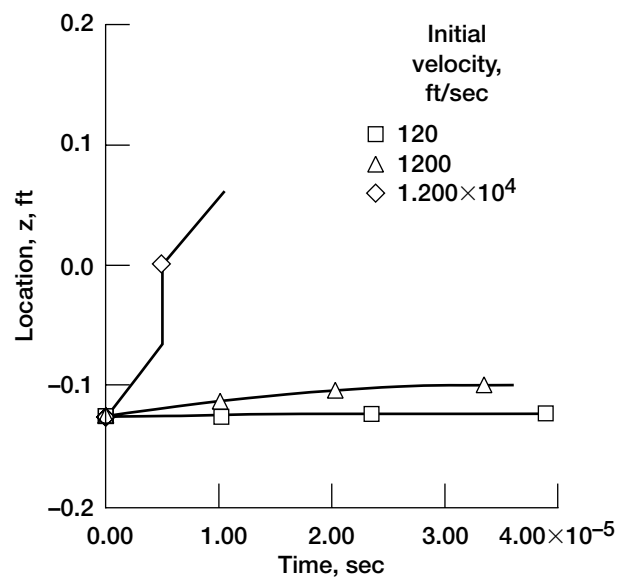graphite/S-glass). (1 lb = 4.45 N, 1 ft = 0.305 m).

Figure 10 – Projective location during impact [0/90/0]$_s$
interply hybrid laminate. (90°-plies intraply hybrid
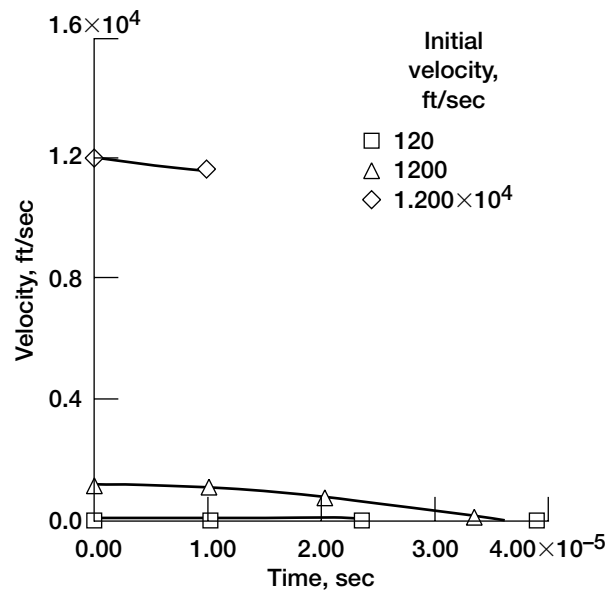graphite/S-glass). (1 in = 2.5 cm; 1 ft = 0.305 m).

Figure 11.—Projectile velocity in a [0/90/0]$_s$ interply hybrid laminate during impact. (90°-plies intraply hybrid graphite/S-glass). (1 ft = 0.305 m).
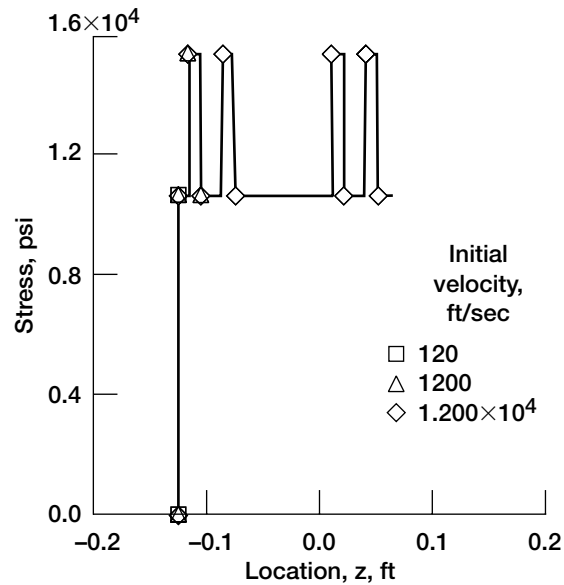

Figure 12.—Interlaminar and intralaminar shear stress developed in [0/90/0]$_s$ interply hybrid laminate during impact (90°-plies intraply hybrid graphite/S-glass). (1 psi = 6.9 Pa).
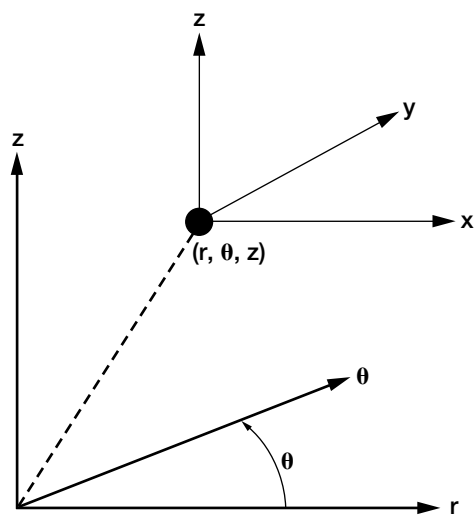
Figure A1.—Coordinate transformation diagram.

REPORT DOCUMENTATION PAGE

Public reporting burden for this collection of information is estimated to average 1 hour per response, including the time for reviewing instructions, searching existing data sources, gathering and maintaining the data needed, and completing and reviewing the collection of information. Send comments regarding this burden estimate or any other aspect of this collection of information, including suggestions for reducing this burden, to Washington Headquarters Services, Directorate for Information Operations and Reports, 1215 Jefferson Davis Highway, Suite 1204, Arlington, VA 22202-4302, and to the Office of Management and Budget, Paperwork Reduction Project (0704-0188), Washington, DC 20503.

1. AGENCY USE ONLY (Leave blank)	2. REPORT DATE	3. REPORT TYPE AND DATES COVERED
	September 2005	Technical Memorandum

4. TITLE AND SUBTITLE

Approximate Micromechanics Treatise of Composite Impact

5. FUNDING NUMBERS

WBS–22–104–08–01

6. AUTHOR(S)

Christos C. Chamis and Louis M. Handler

7. PERFORMING ORGANIZATION NAME(S) AND ADDRESS(ES)

National Aeronautics and Space Administration
John H. Glenn Research Center at Lewis Field
Cleveland, Ohio 44135–3191

8. PERFORMING ORGANIZATION REPORT NUMBER

E–12680–1

9. SPONSORING/MONITORING AGENCY NAME(S) AND ADDRESS(ES)

National Aeronautics and Space Administration
Washington, DC 20546–0001

10. SPONSORING/MONITORING AGENCY REPORT NUMBER

NASA TM—2005-210756

11. SUPPLEMENTARY NOTES

Responsible person, Christos C. Chamis, organization code RO, 216–433–3252.

12a. DISTRIBUTION/AVAILABILITY STATEMENT

Unclassified - Unlimited
Subject Categories: 24 and 39

Available electronically at http://gltrs.grc.nasa.gov

This publication is available from the NASA Center for AeroSpace Information, 301–621–0390.

12b. DISTRIBUTION CODE

13. ABSTRACT *(Maximum 200 words)*

A formalism is described for micromechanic impact of composites. The formalism consists of numerous equations which describe all aspects of impact from impactor and composite conditions to impact contact, damage progression, and penetration or containment. The formalism is based on through-the-thickness displacement increments simulation which makes it convenient to track local damage in terms of microfailure modes and their respective characteristics. A flow chart is provided to cast the formalism (numerous equations) into a computer code for embedment in composite mechanic codes and/or finite element composite structural analysis.

14. SUBJECT TERMS

Penetration; Escape velocity cratering; Coustituents; Failure mechanisms

15. NUMBER OF PAGES

30

16. PRICE CODE

17. SECURITY CLASSIFICATION OF REPORT	18. SECURITY CLASSIFICATION OF THIS PAGE	19. SECURITY CLASSIFICATION OF ABSTRACT	20. LIMITATION OF ABSTRACT
Unclassified	Unclassified	Unclassified	

NSN 7540-01-280-5500

Standard Form 298 (Rev. 2-89)
Prescribed by ANSI Std. Z39-18
298-102